# MATCHING SECTION DESIGN AT THE MeV ULTRAFAST ELECTRON BEAM EXPERIMENTAL FACILITY

H. Qi, C.-Y. Tsai, J. Wang, Z. Z. Liu†, K. J. Fan†
Huazhong University of Science and Technology, Wuhan, China

*Abstract*

This paper introduces the design and optimization of the matching section beamline for the ultrafast electron research platform at Huazhong University of Science and Technology (HUST). The matching section serves as a connection between the main beamline and the beam physics research beamline, aiming to achieve efficient and precise control over the electron beam trajectory and parameters. To evaluate its performance, particle tracking simulations using GPT software were conducted. When the beam is set at 3 MeV and 1 pC charge, the matching section is capable of compressing the bunch length to approximately 50 fs. This level of compression is crucial for ultrafast electron research applications, as it enables the study of phenomena that occur on extremely short time scales, demonstrating its effectiveness in achieving precise beam control and compression.

## INTRODUCTION

The ever increasing demand for high-power and wideband THz radiation has led to its growth in various research fields such as communication [1], biological imaging [2], and plasma diagnostics [3]. To address this demand, we are currently developing a second beamline at HUST that will focus on beam physics research, specifically investigating terahertz radiation and beam Space-Charge (SC) effects.

Figure 1 illustrates the layout of the MeV ultrafast electron beam experimental facility at Huazhong University of Science and Technology (HUST), featuring two beam lines. The primary beamline is dedicated to achieving sub-100 fs time resolution in a MeV ultrafast electron diffraction (UED) setup [4]. The second beamline is connected to the downstream experimental facility through a matching section [5,6], which serves multiple purposes: bending the electron beam and further compressing the bunch.

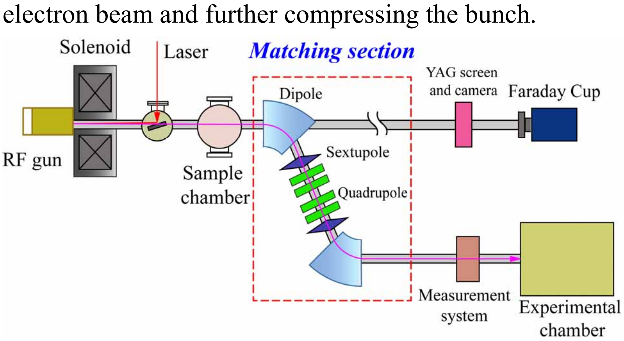


Figure 1: Schematic of the proposed MeV HUST facility.

* Work supported by the National Natural Science Foundation of China (NSFC 12235005 and 12275094), and National key research and development program of China (2022YFA1602202).
† kjfan@hust.edu.cn; † zzliu@hust.edu.cn

Typically, a matching section consists of two dipoles along with quadrupoles and sextupoles that help mitigate dispersion. In the matching section, an electron beam with energy chirp undergoes phase rotation. Through careful design, a positive energy chirp is transformed into a negative chirp, leading to beam compression and ultimately reaching a beam waist downstream. This optimization ensures efficient and compact electron beam propagation.

## BEAM OPTICS DESIGN

During the initial design phase of the matching section, it is typically adequate to consider the first-order beam transport matrix. This matrix, denoted as $R$, describes the transformation of beam parameters from the entrance to the exit of the matching section.

In the matching section, $R$ is composed of the transport matrices of the dipole, quadrupole, and drift elements [7-9]. The linearized form of $R$ can be expressed as follows:

$$R=\begin{bmatrix} R_{11} & R_{12} & 0 & 0 & 0 & R_{16} \\ R_{21} & R_{22} & 0 & 0 & 0 & R_{26} \\ 0 & 0 & R_{33} & R_{34} & 0 & 0 \\ 0 & 0 & R_{43} & R_{44} & 0 & 0 \\ R_{51} & R_{52} & 0 & 0 & 1 & R_{56} \\ 0 & 0 & 0 & 0 & 0 & 1 \end{bmatrix}. \tag{1}$$

The explicit expression of the transport matrix $R$ for the matching section can be obtained by straightforwardly multiplying the transport matrices of each individual element.

Since the matching section serves as a bunch compressor for the second beamline, it is essential to ensure that the energy chirp becomes negative at the exit in order to generate the longitudinal beam waist downstream. This requirement imposes a condition on the transport matrix $R$ of the matching section, specifically that the matrix element $R_{56}$ must be less than zero. Furthermore, the dipole magnets in the matching section introduce a dispersion term that cannot be ignored, which can cause a significant transverse position offset and result in beam loss. To mitigate this issue, dispersion matching becomes necessary, which involves setting the matrix elements $R_{16}$ and $R_{26}$ to zero at the exit of the matching section, effectively eliminating the leakage of dispersion.

The matching section implemented at the HUST experimental facility is designed to be symmetric, and its specific layout is illustrated in Fig. 2. The dipole magnet in this section has a bending angle ($\theta$) of 60 degrees and an effective radius ($\rho$) of 0.26 m. Between the two dipole magnets, four

ISBN: 978-3-95450-265-3 doi:10.18429/JACoW-SAP2023-MOPB016

quadrupoles are strategically positioned to adjust the dispersion term $R_{16}$ and its derivative $R_{26}$. This adjustment aims to minimize the maximum beam size. Additionally, two sextupoles are placed adjacent to the quadrupoles. These sextupoles function as second-order magnet elements but can be considered as drift spaces in terms of first-order optics matching. The lengths of the drifts in the matching section are as follows: L1=0.4 m, L2=0.15 m, L3=0.075 m, D1=0.2 m, and D2=0.1 m, respectively.

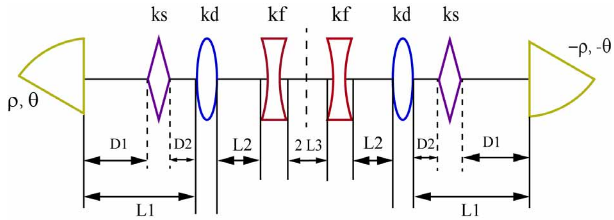


Figure 2: Schematic of the matching section.

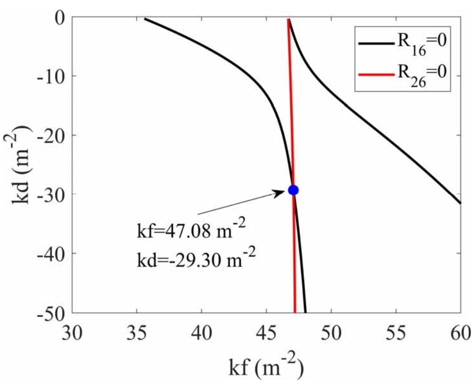


Figure 3: The first-order dispersion ($R_{16}$ and $R_{26}$) as a function of the quadrupole coefficient.

In the first-order optics design of the matching section, we calculate the total transfer matrix $R$. As shown in Fig. 3, by setting the quadrupole coefficients $kf$ =47.08 m$^{-2}$ and $kd$ = -29.30 m$^{-2}$, we achieve $R_{16} = R_{26} = 0$, indicating that the matching section is achromatic at the end of the second dipole. However, this calculation provides a rough approximation as it does not account for the variation of beam parameters (Twiss parameters) within the section. To obtain more accurate results, further analysis is performed using MAD-X software [10]. The matching results are displayed in Fig. 4. In this analysis, the quadrupole coefficients used in the matching section are adjusted to $kf$ = 49.64 m$^{-2}$ and $kd$ = -25.80 m$^{-2}$. Additionally, the longitudinal dispersion $R_{56}$ is determined to be -0.051 m. By applying negative longitudinal dispersion to a positive energy chirp at the entrance of the section, it is possible to generate the longitudinal waist downstream in the second beamline. This configuration allows for the achievement of the minimum bunch length.

The compression section is not purely linear but incorporates higher-order (nonlinear) contributions, which might lead to longitudinal phase space distortion and disruption of the bunch profile. To correct these higher-order terms, multi-pole magnets are typically required. However, for single-pass transport, considering the second-order effect is generally sufficient. In the absence of sextupole magnets, the second-order longitudinal term $T_{566}$ is calculated to be -2.1 m. Two sextupole magnets are employed to mitigate this effect. The sextupoles have opposite polarities and a gradient value of 8.69 T/m$^2$, and the value of $T_{566}$ is reduced to 0, effectively eliminating the second-order term.

By achieving full compression, the downstream beamline can achieve the minimum bunch length. This configuration greatly enhances the quality of the compressed beam.

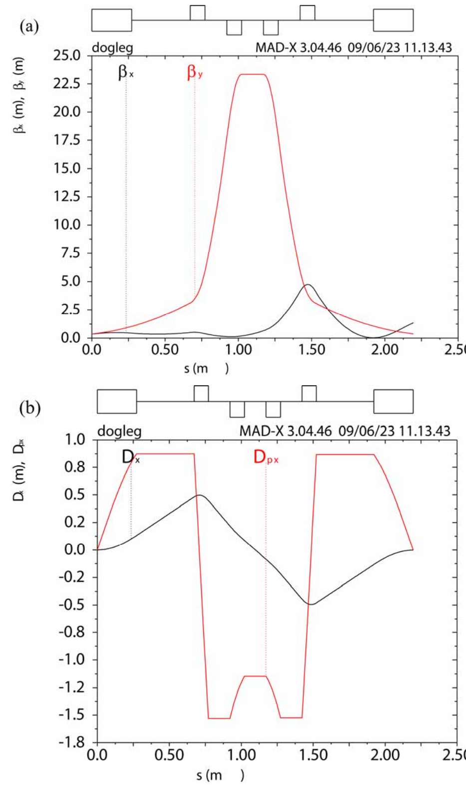


Figure 4: Beam optics in the matching section. The evolution of the (a) betatron function and (b) the first-order dispersion in the section.

## SIMULATION RESULTS

In order to evaluate the efficacy of the lattice design within the matching section, particle tracking simulations that traced the trajectory of particles from the cathode to the downstream region were conducted using the General Particle Tracer (GPT) software [11]. The parameters employed in the simulation are specified in Table 1.

Table 1: Parameters of RF Gun and Solenoid Magnet

| Parameters | Value (unit) |
|---|---|
| Laser spot size | 0.05 mm |
| Laser RMS pulse duration | > 15 fs |
| Beam energy | 3 MeV |
| Injection phase | 65 deg |
| Beam charge | 1 pC |
| Peak field in Solenoid | 0.1445 T |

Figure 5 presents the tracking results obtained under different conditions at two locations: the entrance and down-

ISBN: 978-3-95450-265-3 doi:10.18429/JACoW-SAP2023-MOPB016

stream of the matching section. In Fig. 5(a), the longitudinal phase space and charge density profile at the entrance are depicted. It can be observed that the energy chirp appears to be nearly linear, with a measured value of $h_0$=30.09 m$^{-1}$. Upon passing through the matching section, the chirp undergoes compression, as depicted in Fig. 5(b). However, the absence of sextupoles leads to the formation of a tail in the compressed beam bunch, resulting in an undesirable increase in the bunch length.

To effectively mitigate the impact of the second-order term $T_{566}$ in the beam, sextupole correction is incorporated. This correction significantly improves the tailing behavior of the beam, as illustrated in Fig. 5(c). Consequently, the root mean square (RMS) bunch length can approach approximately 50 fs without the SC effect. However, when the SC effect is taken into account, the RMS bunch length increases to approximately 100 fs due to the interactions between electrons, as shown in Fig. 5(d).

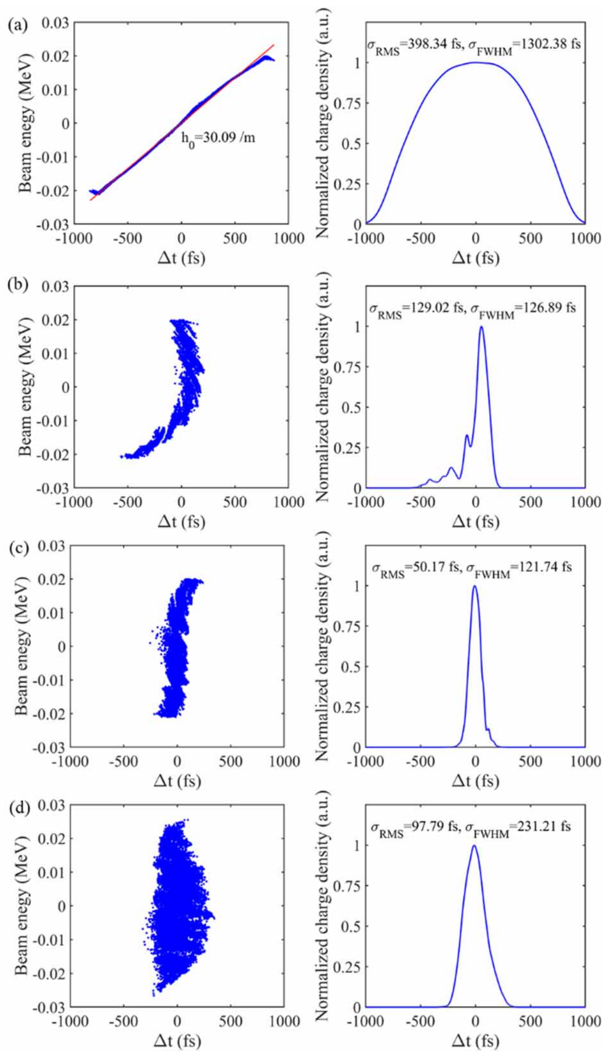


Figure 5: The longitudinal phase space of the beam (left) and its corresponding charge density profile (right), (a) at the entrance of the matching section, and after the matching section tracked (b) without both sextupole correction and SC, (c) with sextupole correction and without SC, and (d) with both sextupole correction and SC incorporated.

Figure 6 illustrates the evolution of beam parameters, specifically the longitudinal bunch length and transverse emittance, as the particles travel from the cathode to the downstream region of the matching section, specifically along the second beamline. Notably, a distinct compression of the bunch length is observed beyond the matching section. However, this compression is accompanied by an increase in the transverse emittance, particularly in the $x$ direction. On the other hand, minimal changes are observed in the $y$ direction.

To further preserve the transverse emittance, precise adjustments to the gradient of the sextupole magnets are necessary, requiring additional efforts. It is crucial to focus on these improvements to optimize the overall performance of the system.

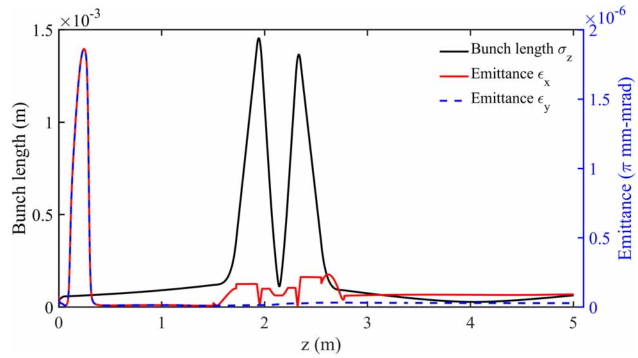


Figure 6: The evolution of beam parameters in the second beamline with SC.

## CONCLUSION

This paper introduces an analytical design of the matching section for a second parallel beamline and subsequently conducts particle tracking simulations to assess its effectiveness and performance. The results demonstrate that the proposed matching section successfully achieves compression of the RMS bunch length, reducing it from 0.4 ps to 50 fs, with an idealistic bunch compression factor of 8. However, when considering the space charge effect, the energy chirp increases, leading to an extension of the RMS bunch length to approximately 100 fs, with a compromised bunch compression factor of 4. Furthermore, the simulations indicate a degradation in the emittance, highlighting the need for further optimization in this aspect. The development of this dual-beam-line configuration, along with the inclusion of the matching section, provides enhanced capabilities for the MeV UED facility at HUST.

## REFERENCES

[1] K. Ishigaki *et al.*, "Direct intensity modulation and wireless data transmission characteristics of terahertz-oscillating resonant tunnelling diodes", *Electron. Lett*, vol. 48, no. 10, pp. 582-583, May 2012. doi:10.1049/el.2012.0849

[2] Z. Yang *et al.*, "Study on an artificial phenomenon observed in terahertz biological imaging", *Biomed. Opt. Express*, vol. 12, no. 6, pp. 3133-3141, Jun. 2021. doi:10.1364/BOE.424445

[3] B. H. Kolner *et al.*, "Plasma characterization with terahertz pulses", *IEEE J Quantum Electron*, vol. 14, no. 2, pp. 505-512, Apr. 2008. doi:10.1109/JSTQE.2007.913395

[4] Y. Song *et al.*, "MeV electron bunch compression and timing jitter suppression using a THz-driven resonator", *Nucl. Instrum. Methods. Phys. Res. A*, vol. 1047, pp. 167774, Feb. 2023. doi:10.1016/j.nima.2022.167774

[5] A. Weinberg and A. Nause, "Dogleg design for an MeV Ultra-fast electron Diffraction beam line for the hybrid Photo-emitted RF GUN at Ariel University", *Nucl. Instrum. Methods. Phys. Res. A*, vol. 989, pp. 164952, Feb. 2021. doi:10.1016/j.nima.2020.164952Z

[6] R. J. England *et al.*, "Beam shaping and compression scheme for the UCLA Neptune Laboratory", in *Proc. 2003 Particle Accelerator Conf. (PAC2003)*, Portland, OR, May 2003, p. 3258. doi:10.1109/PAC.2003.1289880

[7] A. Wolski, "Beam dynamics in high energy particle accelerators", World Scientific, 2014.

[8] C.-Y. Tsai *et al.*, "Low-energy high-brightness electron beam dynamics based on slice beam matrix method", *Nucl. Instrum. Methods. Phys. Res. A*, vol 937, pp. 1-20, Sep. 2019. doi:10.1016/j.nima.2019.05.035

[9] C.-Y. Tsai and K. Fan, "A Semi-Analytical Approach to Six-Dimensional Path-Dependent Transport Matrices With Application to High-Brightness Charged-Particle Beam Transport", in *Proc. 2019 North American Particle Acc. Conf. (NAPAC2019)*, Lansing, MI, US, Sep. 2019, pp. 792-795. doi:10.18429/JACoW-NAPAC2019-WEPLS12

[10] H. Grote and F. Christoph Iselin, "User's Reference Manual for the MAD-X Program", version 5.08.01, Geneva, Switzerland, Feb. 2022.

[11] General Particle Tracer, http://www.pulsar.nl/gpt.